

## Article

# Treatment of Coking Wastewater by $\alpha$ -MnO<sub>2</sub>/Peroxymonosulfate Process via Direct Electron Transfer Mechanism

Jia Wang<sup>1,2,\*,†</sup>, Zhuwei Liao<sup>3,†</sup>, Jiayi Cai<sup>4</sup>, Siqi Wang<sup>2</sup>, Fang Luo<sup>2</sup>, Jerosha Ifthikar<sup>2</sup>, Songlin Wang<sup>1</sup>, Xinquan Zhou<sup>5,\*</sup> and Zhuqi Chen<sup>1,2,\*</sup>

<sup>1</sup> School of Environmental Science and Engineering, Huazhong University of Science and Technology, Wuhan 430074, China

<sup>2</sup> Key Laboratory of Material Chemistry for Energy Conversion and Storage, Ministry of Education, Hubei Key Laboratory of Material Chemistry and Service Failure, School of Chemistry and Chemical Engineering, Huazhong University of Science and Technology, Wuhan 430074, China

<sup>3</sup> Department of Environmental Engineering, Urban Construction Engineering Division, Wenhua College, Wuhan 430074, China

<sup>4</sup> Ecological and Environmental Monitoring and Scientific Research Center, Ecology and Environment Administration of Yangtze River Basin, Ministry of Ecology and Environment, Wuhan 430010, China

<sup>5</sup> School of Chemical Engineer and Pharmacy, Henan University of Science and Technology, Luoyang 471000, China

\* Correspondence: jiawang@hust.edu.cn (J.W.); 9906240@haust.edu.cn (X.Z.); zqchen@hust.edu.cn (Z.C.); Tel.: +86-13476079416 (Z.C.)

† These authors contributed equally to this work.



**Citation:** Wang, J.; Liao, Z.; Cai, J.; Wang, S.; Luo, F.; Ifthikar, J.; Wang, S.; Zhou, X.; Chen, Z. Treatment of Coking Wastewater by  $\alpha$ -MnO<sub>2</sub>/Peroxymonosulfate Process via Direct Electron Transfer Mechanism. *Catalysts* **2022**, *12*, 1359. <https://doi.org/10.3390/catal12111359>

Academic Editors: Jiangkun Du, Lie Yang and Chengdu Qi

Received: 10 October 2022

Accepted: 24 October 2022

Published: 3 November 2022

**Publisher's Note:** MDPI stays neutral with regard to jurisdictional claims in published maps and institutional affiliations.



**Copyright:** © 2022 by the authors. Licensee MDPI, Basel, Switzerland. This article is an open access article distributed under the terms and conditions of the Creative Commons Attribution (CC BY) license (<https://creativecommons.org/licenses/by/4.0/>).

**Abstract:** Side reactions between free radicals and impurities decelerate the catalytic degradation of organic contaminants from coking wastewater by Advanced Oxidation Processes (AOPs). Herein, we report the disposal of coking wastewater by  $\alpha$ -MnO<sub>2</sub>/PMS process via a direct electron transfer mechanism in this study. By the removal assays of the target compound of phenol, the PMS mediated electron transfer mechanism was identified as the dominated one. Water quality parameters including initial pH, common anions and natural organic matters demonstrated limited influences on phenol degradation. Afterwards,  $\alpha$ -MnO<sub>2</sub>/PMS process was applied on the disposal of coking wastewater. The treatment not only eliminated organic contaminants with COD removal of 73.8% but also enhanced BOD<sub>5</sub>/COD from 0.172 to 0.419, within 180 min of reaction under conditions of 50 g/L  $\alpha$ -MnO<sub>2</sub>, 50 mM PMS and pH<sub>0</sub> 7.0. COD removal decreased only 1.1% after five-time cycle application, suggesting a good reuse performance. A quadratic polynomial regression model was further built to optimize the reaction conditions. By the model, the dosage of  $\alpha$ -MnO<sub>2</sub> was identified as the most important parameters to enhance the performance. The optimal reaction conditions were calculated as 50 g/L  $\alpha$ -MnO<sub>2</sub>, 50 mM PMS and pH<sub>0</sub> 6.5, under which COD removal of 74.6% was predicted. All aforementioned results suggested that the  $\alpha$ -MnO<sub>2</sub>/PMS process is a promising catalytic oxidation technology for the disposal of coking wastewater with good practical potentials.

**Keywords:** alpha manganese dioxide; peroxymonosulfate; electron transfer; catalytic oxidation; coking wastewater

## 1. Introduction

Coal is the most important energy resource in China because it accounts for at least 70% of China's energy consumption [1]. Coking wastewater generates from coal coking, by-products recovery, refinement processes and coal gas purification in coal plants [2]. To yield 1 ton of coal, 0.31–4.00 m<sup>3</sup> of coking wastewater is reported to be produced [3,4]. At present, approximately 0.3 billion tons of coking wastewater is generated every year in China [5]. In view of the whole world, the yield is 0.75 billion tons per year [4]. The discharged Chemical Oxygen Demand (COD) from coking wastewater every year accounts for more than 1.5% of that from the total wastewater [5]. More importantly, it is one of the most

cumbersome wastewaters handled by human beings, being typically characterized by high toxicity, low biodegradability, high nitrogen and COD concentrations, as well as its complex compositions [6]. Thus, coking wastewater emerges as an on-going challenge in the field of wastewater treatment [7]. The development for the disposal of coking wastewater attracts a lot of attentions [8].

Coking water contains organic contaminants involving phenols, pyrrole, furan, naphthalene, polycyclic aromatic hydrocarbon and other refractory components [9,10]. China issued a strict discharge standard for coking wastewater (GB 16171-2012) [11]. Treatment of coking wastewater has become more and more sophisticated, evolving from simple mechanical approaches prevalent during the 1950s to 1960s to the boom of biochemical technology during the 1980s to 1990s [12]. However, disposed by biochemical technologies, coking wastewater may not meet the discharge standard due to its low biodegradability: non-biodegradable constituents account for over 40% of total organic compounds, and also large amounts of refractory organics [5,13]. In addition, disadvantages including low efficiency, unstable operation and potential second pollutions have impeded the practical applications of other traditional technologies such as physicochemical ones [14,15]. In the last decade, Advanced Oxidation Processes (AOPs) have emerged as one of the most promising technologies for the elimination of organic contaminants in coking wastewater [16,17]. For instance, homogeneous AOPs were reported to be efficient in disposing of coking wastewater. For example, Fenton oxidation treatment was reported to achieve COD, phenol and cyanide removal of 84.66%, 88.46% and 79.34%, respectively, in coking wastewater [18]. In another case, a the Fenton-denitrification process was employed to eliminate both organic contaminants and total nitrogen [19]. However, drawbacks including the narrow pH window of the reaction and quenching of reactive oxygen species (ROS) by a homogeneous activator limited their applications. Thus, heterogeneous AOPs were employed in more cases. For instance, manganese oxide ore acidic oxidation was employed to efficiently degrade the organic contaminants in coking wastewater [20]. In another study, a process of  $O_3/H_2O_2/Fe$ -shavings, which coupled catalytic ozonation and Fenton-like oxidation with Fe-shaving wastes reused, demonstrated high efficiency in the treatment of coking wastewater secondary biochemical effluent [11]. Unfortunately, due to the strong quenching effects of impurities on ROS, especially free radicals, huge amounts of reaction reagents and power were consumed to achieve high efficiency. Even worse, the disposal performance was not that stable due to the variable physicochemical properties of coking wastewater. Inorganic pollutants including sulfate, chlorides, cyanides and nitrides are widely dispersed in coking wastewater [11]. In addition, coking wastewater is characterized by its high alkalinity and hardness [14]. In all homogeneous AOPs and even some heterogeneous ones, the elimination efficiencies of contaminants varied extensively with changeable water matrix parameters such as reaction pHs, natural organic matter (NOM) and anions [21,22]. Furthermore, a human carcinogen was widely reported to be generated via the oxidation of  $Br^-$  by free radicals in AOPs [21,23]. The complications in removing the refractory organics and the inhibitory effects of inorganic compounds are stumbling blocks for the effective disposal of coking wastewater.

To overcome the aforementioned limitations, a heterogeneous system with stable performance and degradation products in low toxicity was eagerly desired. Sulfate radicals-based AOPs (SR-AOPs) were widely employed due to the high stability that benefits the storage and transportation, wide reactivity with contaminants and relatively lower cost demand [24–29]. In some peroxymonosulfate (PMS)-based systems, non-radical species such as singlet oxygen [30–32], metastable PMS [33–35] and non-radical routes such as direct electron transfer from pollutants to PMS [36,37] were reported to dominate the removal of organic contaminants. In such systems, side reactions between free radicals and the co-existing inorganic impurities could be avoided [38,39].  $MnO_2$  was widely employed as highly efficient PMS activator [40,41]. The mechanism of organic degradation was highly dependent on its crystal facets [42]. Very recently, we disclosed the underlying mechanism of PMS activation by a series of crystallographic  $MnO_2$  as oxidation by surface bound

metastable PMS and direct electron transfer from organic contaminants to surface Mn(IV, III) [34]. We employed the most reactive one,  $\alpha$ -MnO<sub>2</sub>, as a PMS activator towards the disposal of coking wastewater in this study. In our research hypothesis, refractory contaminants would be highly-efficiently degraded via non-radical pathways, with low dosages of reaction reagents and negligible influences from impurities in wastewater. Inspired by the advantage of quickly analyzing the interactions between multiple parameters, optimizing and predicting the experimental parameters with a low number of experiments, the response surface method (RSM) was employed to optimize the reaction conditions of the  $\alpha$ -MnO<sub>2</sub>/PMS process [11,13]. Due to the fact that phenols were reported to account for more than 80% of the total COD in coking wastewater [14], we chose phenol as the model compound to uncover the mechanism of our system to degrade organic contaminants. By the aforementioned efforts, we aim to propose a strategy to treat coking wastewater via a non-radical mechanism by the  $\alpha$ -MnO<sub>2</sub>/PMS process and evaluate its potential practical applications.

## 2. Results and Discussion

### 2.1. Degradation of Phenol by $\alpha$ -MnO<sub>2</sub>/PMS Process

Before the experiments of phenol degradation, the successful synthesis of  $\alpha$ -MnO<sub>2</sub> was confirmed by scanning electron microscope (SEM, Figure S1) and X-ray diffraction (XRD, Figure S2). Initial assays were carried out to test the removal of phenol by only  $\alpha$ -MnO<sub>2</sub>, only PMS or  $\alpha$ -MnO<sub>2</sub>/PMS system (Figure 1A). Only 5.9% of phenol was removed via adsorption by  $\alpha$ -MnO<sub>2</sub>, suggesting that the adsorption capacity of  $\alpha$ -MnO<sub>2</sub> was low. In our previous study, the surface area of  $\alpha$ -MnO<sub>2</sub> was demonstrated as 34.1 m<sup>2</sup>/g [34]. The sluggish adsorption of phenol was most likely attributed to the low surface area of  $\alpha$ -MnO<sub>2</sub>. A lower phenol removal of 2.2% was achieved only in the PMS group. This result was consistent with previous studies, suggesting that PMS was obtuse to degrade refractory organic compounds without activation [26,43,44]. Phenol removal dramatically increased to 99.3% when  $\alpha$ -MnO<sub>2</sub> was introduced only into the PMS group, suggesting that  $\alpha$ -MnO<sub>2</sub> successfully activated PMS.

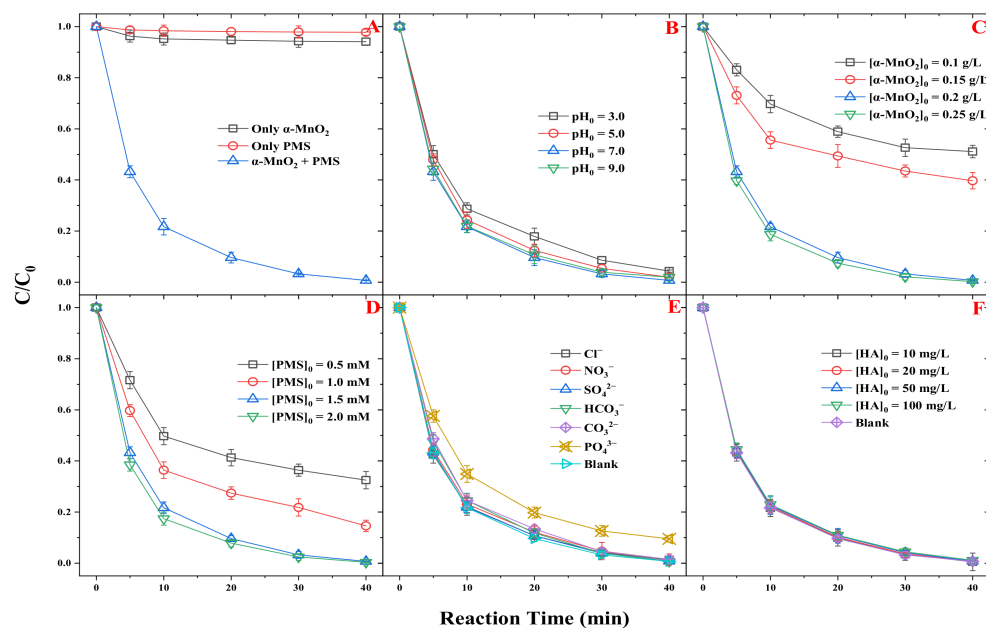
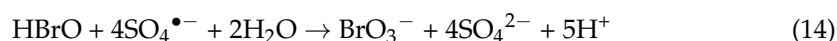
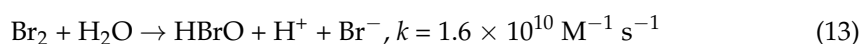
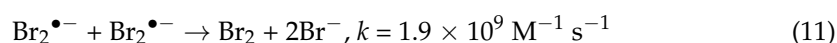
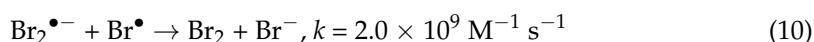
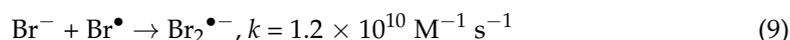
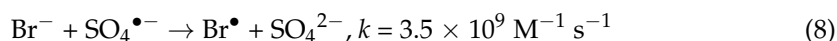
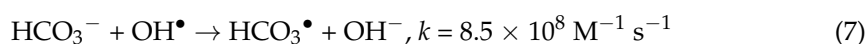
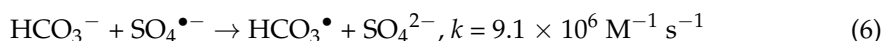
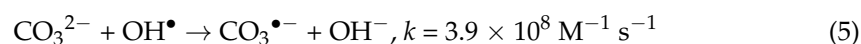
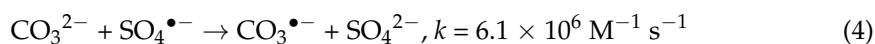
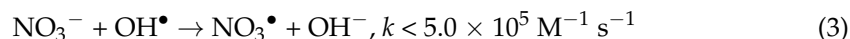
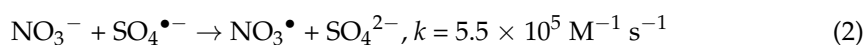
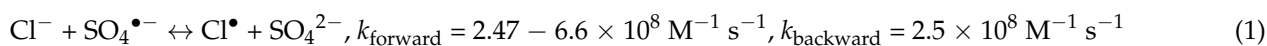


**Figure 1.** Removal of phenol by only  $\alpha$ -MnO<sub>2</sub>, only PMS or  $\alpha$ -MnO<sub>2</sub>/PMS system (A), effects of pH (B),  $\alpha$ -MnO<sub>2</sub> dosage (C), PMS dosage (D), common anions (E) and HA concentration (F) on phenol removal by  $\alpha$ -MnO<sub>2</sub>/PMS system. Reaction conditions:  $[\alpha\text{-MnO}_2]_0 = 0.2$  g/L,  $[\text{PMS}]_0 = 1.5$  mM,  $[\text{phenol}]_0 = 20$  mg/L,  $\text{pH}_0 = 7.0$ , Temperature = 30 °C,  $[\text{anions}]_0 = 5.0$  mM.

Effects of initial pH on phenol removal were then evaluated (Figure 1B). Along with the initial pH increase from 3.0 to 7.0, phenol removal increased from 95.7% to 99.3%. When the initial pH further increased to 9.0, phenol removal decreased to 98.1%. The pH-independent performance was consistent with that in our previous work which employed manganese anode slag as the PMS activator [45]. The aforementioned results can be attributed to two reasons. Firstly, PMS mainly exists as  $\text{HSO}_5^-$  at  $\text{pH}_0$  3.0 and 5.0 and the stabilization effect between  $\text{HSO}_5^-$  and  $\text{H}^+$  might reduce the effective activation of PMS [46]. Then, point of zero charge ( $\text{pH}_{\text{PZC}}$ ) of  $\alpha\text{-MnO}_2$  was determined to be 7.9 (Figure S3). At a  $\text{pH}_0$  of 9.0, the electro-negative surface of  $\alpha\text{-MnO}_2$  is not conducive to the contact of  $\text{HSO}_5^-$  and  $\text{SO}_5^{2-}$  [26]. Electron transfer was identified as one of the major mechanisms to degrade phenol in our system (*vide infra* in Section 2.2); thus, ineffective contact between PMS and  $\alpha\text{-MnO}_2$  might delay the degradation of phenol [47]. Since that even at  $\text{pH}_0$  3.0, 95.7% of phenol was eliminated, we concluded that the influence of the initial pH on the performance of the  $\alpha\text{-MnO}_2$ /PMS system was weak. Furthermore, the concentration of leached Mn at  $\text{pH}_0$  3.0, 5.0, 7.0 and 9.0 was revealed as 0.15, 0.07, 0.02 and 0.01 ppm, respectively (Figure S4), which were far below the highest limit in Chinese Integrated Wastewater Discharge Standard (GB8978-1996) and Sanitary Standard in China for Drinking Water (GB5749-2006) [45]. The results suggested that the  $\alpha\text{-MnO}_2$ /PMS process uses a green strategy to eliminate organic contaminants without the second pollution of metal leaching.

Then, the effects of  $\alpha\text{-MnO}_2$  (Figure 1C) and PMS (Figure 1D) dosages were studied. Phenol removal increased from 48.9% to 99.8% along with the increase in  $\alpha\text{-MnO}_2$  dosage from 0.1 to 0.25 g/L. With respect to PMS dosage, along with its increase from 0.5 to 2.0 mM, phenol removal increased from 67.5% to 99.7%. The results suggested that with higher dosages of  $\alpha\text{-MnO}_2$  or PMS, we could achieve higher phenol removal. The increase in phenol removal with higher  $\alpha\text{-MnO}_2$  dosage was attributed to additional reactive sites for catalytic reactions [28]. The increase with higher PMS dosage was attributed to more frequent contact between PMS and reactive sites [25].

The impacts of common anions on phenol degradation were further disclosed (Figure 1E). Most anions demonstrated limited influence since phenol removal of 98.7%, 98.6%, 99.2%, 99.3%, 98.5% was achieved in the presence of 5.0 mM of  $\text{Cl}^-$ ,  $\text{NO}_3^-$ ,  $\text{SO}_4^{2-}$ ,  $\text{HCO}_3^-$  and  $\text{CO}_3^{2-}$ , respectively. Free radicals including sulfate radicals ( $\text{SO}_4^{\bullet-}$ ,  $E^0 = 2.5\text{--}3.1$  V) and hydroxyl radicals ( $\text{OH}^{\bullet}$ ,  $E^0 = 1.9\text{--}2.7$  V) were reported to be transferred to radicals with lower reactivity such as nitrate radicals ( $\text{NO}_3^{\bullet}$ ,  $E^0 = 2.0\text{--}2.2$  V) in the presence of the aforementioned anions (Equations (1)–(7)) [24,48,49]. Based on this fact, the degradation reaction should be partly decelerated. The unusual phenomena should be attributed to two reasons. Firstly, in the case of  $\text{Cl}^-$ , the quenching reaction (Equation (1)) was reported to be reversible and the rate constants of the forward and reverse pathway are similar [48]. Under a high concentration of  $\text{SO}_4^{\bullet-}$ , certain amounts of  $\text{SO}_4^{\bullet-}$  was quenched, which may help to avoid its self-quenching. Under a low concentration, the reverse pathway will undergo, which may facilitate the regeneration of  $\text{SO}_4^{\bullet-}$  and maintain the reaction efficiency [24]. Secondly, according to the non-radical dominated mechanism (*vide infra* in Section 2.2), free radicals did not contribute too much to phenol degradation. Thus, the quenching effects of free radicals by common anions were negligible in this case, while, in the presence of  $\text{PO}_4^{3-}$ , phenol removal significantly decreased to 90.5%. This phenomenon was attributed to the inhibition effects on the formation of surface-bound PMS complex due to the substitution of surface hydroxyl groups by phosphate [33,50,51]. The formation of  $\text{BrO}_3^-$  was further tested in the presence of  $\text{Br}^-$  (Figure S5).  $\text{BrO}_3^-$  was reported to be formatted via the chain reactions between  $\text{Br}^-$  and free radicals such as sulfate radicals (Equations (8)–(14)) [21,52]. In a typical free radicals-based system, Mn(II)/PMS, 1.27 mM of  $\text{BrO}_3^-$  was formatted, while in  $\alpha\text{-MnO}_2$ /PMS system, the concentration of  $\text{BrO}_3^-$  during the whole reaction was under the detection limit. The results suggested that it was favored by the non-radical dominated mechanism, no  $\text{BrO}_3^-$ , which is a potent carcinogen subjected to strict regulation globally, generated in  $\alpha\text{-MnO}_2$ /PMS system.



The effects of Natural Organic Matters (NOMs) on phenol removal were disclosed with humic acid (HA) as representative NOMs. Phenol removal was tested as 99.5%, 99.3%, 99.2% and 98.9% in the presence of 10, 20, 50 and 100 mg/L HA, respectively. The results suggested that nearly no effects of HA on phenol removal, which was significantly distinguished with phenomena in free radicals-based systems [25,27]. The result suggested that the  $\alpha$ -MnO<sub>2</sub>/PMS process is a promising approach for the treatment of real wastewaters with a high amount of background organic matter. To further evaluate the effects of water matrices, phenol removal was tested in tap water and lake water (Figure S6). We found that similar phenol removal of 99.1% was achieved in tap water. Even in lake water with a higher concentration of impurities, a satisfying phenol removal of 98.2% was achieved.

All aforementioned results suggested that PMS was successfully activated by  $\alpha$ -MnO<sub>2</sub>. More importantly, the performance of the  $\alpha$ -MnO<sub>2</sub>/PMS system remained highly efficient and stable in complex water matrices.

## 2.2. Non-Radical Mechanism of $\alpha$ -MnO<sub>2</sub>/PMS Process

To identify the dominated reactive oxidative species (ROS) in  $\alpha$ -MnO<sub>2</sub>/PMS system, quenching studies were firstly carried out (Figure 2A). Methanol (MeOH) was employed as the scavenger of  $\text{SO}_4^{\bullet-}$  ( $k = 2.5 \times 10^7 \text{ M}^{-1} \text{ s}^{-1}$ ) and also  $\text{OH}^\bullet$  ( $k = 9.7 \times 10^8 \text{ M}^{-1} \text{ s}^{-1}$ ) [25]. Tert-butyl alcohol (TBA) was employed as the scavenger of  $\text{OH}^\bullet$  ( $k = 6.0 \times 10^8 \text{ M}^{-1} \text{ s}^{-1}$ ) [27]. Furfuryl alcohol (FFA) was applied as the scavenger of singlet oxygen ( $^1\text{O}_2$ ,  $k = 1.2 \times 10^8 \text{ M}^{-1} \text{ s}^{-1}$ ) [53].  $\text{CO}_3^{2-}$  (20 mM) was employed as the scavenger of superoxide radicals ( $\text{O}_2^{\bullet-}$ ,  $k = 5.0 \times 10^8 \text{ M}^{-1} \text{ s}^{-1}$ ) [54]. Phenol removal was demonstrated as 98.7%, 99.1%, 98.9% and 98.8% in the presence of 1000 mM MeOH, 1000 mM TBA, 2 mM FFA and 20 mM  $\text{CO}_3^{2-}$ , which was similar as that without any scavenger. The phenomena suggested that all common ROS including  $\text{SO}_4^{\bullet-}$ ,  $\text{OH}^\bullet$ ,  $^1\text{O}_2$  and  $\text{O}_2^{\bullet-}$  did not participate in the degradation of phenol. Electron paramagnetic resonance (EPR) experiments with 5,5-dimethylpyrrolineN-oxide (DMPO) and 2,2,6,6-tetramethyl-4-piperidinol (TEMP) as spin-trapping reagents were further conducted to confirm the conclusion. As illustrated in Figure 2B, both the signals DMPO- $\text{SO}_4^{\bullet-}$  and DMPO- $\text{OH}^\bullet$  remained silent, ruling free radicals as major ROS again. Surprisingly, in the group of  $\alpha$ -MnO<sub>2</sub>/PMS, a typical heptet signal with special hyperfine splitting constants of  $\alpha_{\text{N}} = 7.3 \pm 0.1 \text{ G}$  and  $\alpha_{\text{H}} = 3.9 \pm 0.1 \text{ G}$

was found, indicating the generation of 5,5-dimethyl-1-pyrrolidone-2-oxyl (DMPOX) [55]. DMPOX was widely reported to be generated via direct oxidation of DMPO in the absence of free radicals [56,57]. In the case employed TEMP as the spin-trapping reagent, no signal of TEMP- $^1\text{O}_2$  was detected (Figure 2C). Phenol removal assays were also carried out in  $\text{D}_2\text{O}$  (Figure S7). Additionally, 99.5% of phenol was removed following a first-order kinetic model with the rate constant of  $0.123 \text{ min}^{-1}$ , which was consistent with the removal (99.3%) and rate constant ( $0.119 \text{ min}^{-1}$ ) in deionized water. The half-life of  $^1\text{O}_2$  in  $\text{D}_2\text{O}$  is almost 10 times higher than that in deionized water, while the removal of organic contaminants in  $^1\text{O}_2$  dominated systems was reported to be accelerated [58]. The EPR spectra and results in  $\text{D}_2\text{O}$  experiments ruled out  $^1\text{O}_2$  as major ROS again. Very recently, high-valent metal-oxo species emerged as a novel ROS to degrade organic contaminants [59]. Via the oxidation by high-valent metal-oxo species through oxygen transfer, methyl phenyl sulfoxide (PMSO) could correspond to sulfone product and methyl phenyl sulfone ( $\text{PMSO}_2$ ) [60]. Thus, the PMSO oxidation experiments were carried out (Figure 2D). Large amount of PMSO was consumed ( $60.2 \mu\text{M}$ ); however, no  $\text{PMSO}_2$  was generated. Thus, we can conclude that high-valent metal-oxo species did not participate in the degradation of phenol in this case.

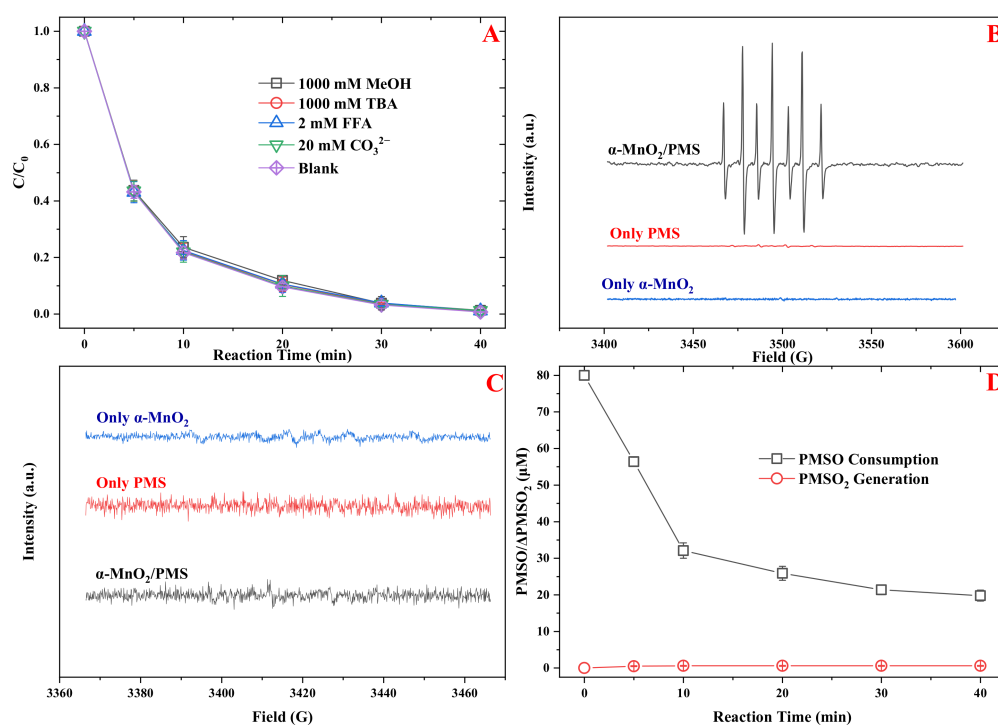


**Figure 2.** Effects of various ROS quencher on phenol removal (A), EPR spectra in the presence of DMPO (B), EPR spectra in the presence of TEMP (C) and PMSO consumption and  $\text{PMSO}_2$  generation in  $\alpha\text{-MnO}_2/\text{PMS}$  system (D). Reaction conditions:  $[\alpha\text{-MnO}_2]_0 = 0.2 \text{ g/L}$ ,  $[\text{PMS}]_0 = 1.5 \text{ mM}$ ,  $[\text{phenol}]_0 = 20 \text{ mg/L}$ ,  $\text{pH}_0 = 7.0$ , Temperature =  $30 \text{ }^\circ\text{C}$ .

Based on the aforementioned phenomena that all common ROS did not contribute to phenol degradation, a direct electron transfer mechanism was considered by us. The mediated electron transfer reaction occurs when PMS and organic pollutants simultaneously participate in the reaction, while the ROS generation could be triggered in the absence of organic contaminants [61]. Thus, to further disclose the degradation mechanism of phenol, PMS decomposition was firstly measured (Figure 3A). In the absence of phenol, 2.9% of PMS was decomposed. After injection of phenol into the reaction, PMS decomposition increased from 18.9% to 47.3% along with the increased amounts of injected phenol from 5 to 20 mg/L. The phenomena clearly indicated that pollutants remarkably promoted the electron transfer process in  $\alpha\text{-MnO}_2/\text{PMS}$  system [62]. The chronoamperometric electrochemical measurements further elucidated the electron transfer mechanism (Figure 3B). No

significant change in current was observed after the addition of PMS at 100 s in the i-t curve. However, the current changed dramatically after the addition of phenol at 200 s, indicating that PMS and phenol acted as electron acceptor and donor, respectively, on the surface of  $\alpha$ -MnO<sub>2</sub> to trigger the electron transfer reaction, which was consistent with the PMS decomposition experiment [63]. For gain further insight into the PMS mediated electron transfer mechanism, the effects of phosphate at a higher concentration on phenol removal were studied (Figure 3C). Phenol removal rapidly decreased from 99.3% to 87.2%, 79.2%, 57.8% and 47.1% when phosphate concentration increased from 0 to 10, 20, 50 and 100 mM, respectively. It is well known that surface hydroxyl groups were readily substituted by phosphate, thereby inhibiting the formation of surface-bound PMS complexes [33]. The results suggested that surface hydroxyl groups are major adsorption sites for PMS in the electron transfer process.

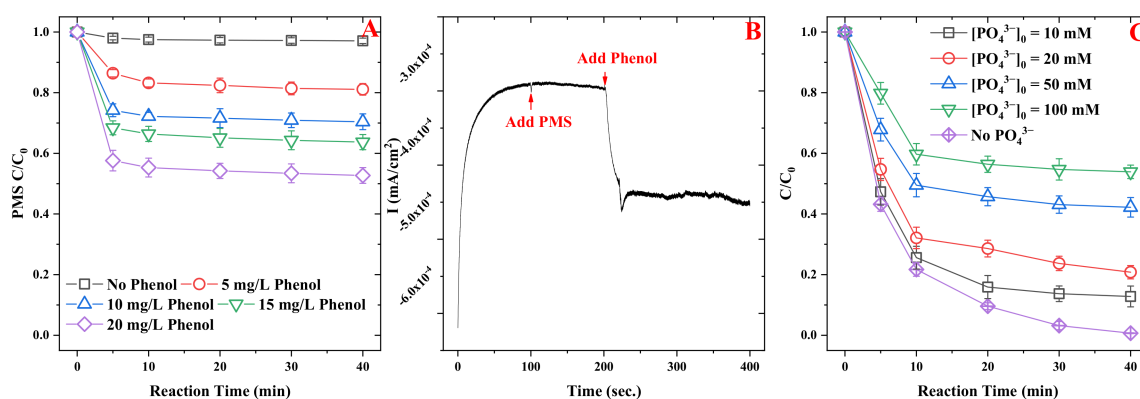


**Figure 3.** Decomposition of PMS in the presence of various concentrations of phenol (A), i-t curve of  $\alpha$ -MnO<sub>2</sub> (B), degradation of phenol in the presence of higher concentration of PO<sub>4</sub><sup>3-</sup> (C). Reaction conditions: [ $\alpha$ -MnO<sub>2</sub>]<sub>0</sub> = 0.2 g/L, [PMS]<sub>0</sub> = 1.5 mM, [phenol]<sub>0</sub> = 0–20 mg/L, pH<sub>0</sub> = 7.0, [PO<sub>4</sub><sup>3-</sup>]<sub>0</sub> = 0–100 mM Temperature = 30 °C.

In summary, all aforementioned data identified PMS mediated electron transfer as the dominated mechanism for phenol degradation.

### 2.3. Disposal of Coking Wastewater by $\alpha$ -MnO<sub>2</sub>/PMS Process

Since the  $\alpha$ -MnO<sub>2</sub>/PMS process demonstrated a satisfying performance in the removal of phenol, it has good potential to eliminate organic contaminants from coking wastewater. Thus, further efforts were paid to study its performance on the disposal of coking wastewater. Firstly, COD removal was measured (Figure 4A). Only  $\alpha$ -MnO<sub>2</sub> and only PMS performed very sluggishly, with COD removal of 1.4% and 1.8%, respectively. In the  $\alpha$ -MnO<sub>2</sub>/PMS process, 73.8% of COD was removed within 180 min of reaction. Mn(II)/PMS, a typical free radicals-based system, was performed as a comparison. Only 25.3% of COD was removed in the Mn(II)/PMS system. The results indicated that the non-radical  $\alpha$ -MnO<sub>2</sub>/PMS process was more efficient and robust in the disposal of real wastewater, with a high concentration of interfering substances. Considering that biochemical technologies are combined with AOPs in some cases to guarantee that the water quality of effluent can reach the discharge standard [6], the performance of the  $\alpha$ -MnO<sub>2</sub>/PMS process to enhance the biodegradability index (BOD<sub>5</sub>/COD) was further tested (Figure 4B). BOD<sub>5</sub>/COD of the original sample, the sample only in  $\alpha$ -MnO<sub>2</sub>, only PMS and Mn(II)/PMS groups were tested as low as 0.172, 0.175, 0.181 and 0.268, respectively. The value increased significantly to 0.419 after treatment by the  $\alpha$ -MnO<sub>2</sub>/PMS process. The results suggested that organic compounds which are refractory to biodegradation were efficiently degraded into intermediates with higher biodegradability [64]. To further confirm the practical potentials of the  $\alpha$ -MnO<sub>2</sub>/PMS process, reuse performance of  $\alpha$ -MnO<sub>2</sub> was evaluated (Figure 4C). The performance was nearly consistent in the five-cycle application because 73.8%, 73.4%,

73.6%, 72.9% and 72.7% of COD was removed in the first, second, third, fourth and fifth run of the  $\alpha$ -MnO<sub>2</sub>/PMS process. The good reuse performance was widely reported in AOPs dominated by direct electron transfer mechanism due to the fact that little change in the structure of the heterogeneous catalysts occurred during the activation [65,66].

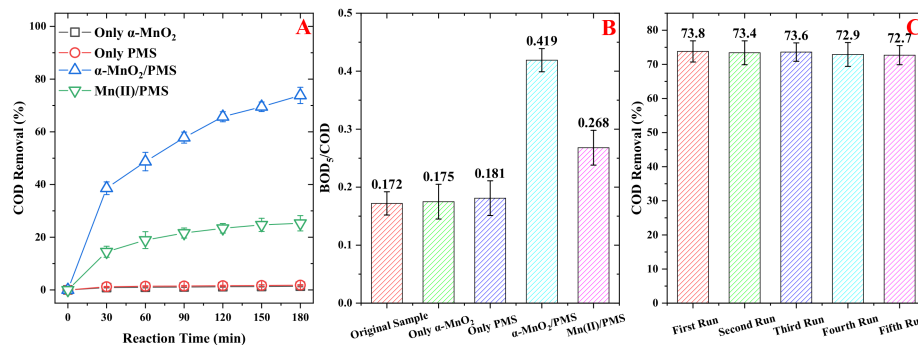


**Figure 4.** Removal of COD from coking wastewater (A), enhancement of the biodegradability index (B), and the reuse performance of  $\alpha$ -MnO<sub>2</sub>/PMS process (C). Reaction conditions:  $[\alpha$ -MnO<sub>2</sub>]<sub>0</sub> = 50 g/L, [Mn(II)]<sub>0</sub> = 50 mM, [PMS]<sub>0</sub> = 50 mM, pH<sub>0</sub> = 7.0, Temperature = 30 °C.

We further studied the effects of reaction conditions including the dosage of catalyst ( $X_1$ ), the dosage of PMS ( $X_2$ ) and initial pH ( $X_3$ ) on COD removal ( $Y$ ) by the results of seventeen sets of single-factor experiments (Table S1). The experimental results were fitted by polynomial regression, and a quadratic polynomial regression model was fitted to predict the COD removal, as shown in Equation (15).

$$Y = 1.44354 X_1 + 0.15375 X_2 - 4.05526 X_3 - 0.00767 X_1 X_2 - 0.00083 X_1 X_3 + 0.05722 X_2 X_3 + 0.00018 X_1^2 + 0.00994 X_2^2 + 0.21757 X_3^2 + 8.32209 \quad (15)$$

ANOVA analysis was employed to analyze the significance and adequacy of the experimental data (Table 1) [11].  $F$  value and  $p$  value were 17.451 and 0.0005, respectively, indicating that aforementioned model was statistically significant [67].  $F$  value and  $p$  value of the lack of fit was 7.660 and 0.2164, indicating that the term was not significant. To further test the significance of the model, error statistical analysis was performed on the fitted regression equations (Table 2). The multivariate correlation coefficient ( $R^2$ ) and the adjusted determination correlation coefficient (adj- $R^2$ ) of the model was as high as 98.74% and 96.26%, respectively, verifying the significance of the model [13]. The low coefficient of variation (C.V.) was as low as 3.7%, indicating the high accuracy and reliability of the model [68].  $F$  value of  $X_1$ ,  $X_2$  and  $X_3$  was 131.051, 79.751 and 22.955, while  $p$  value was <0.0001, 0.0008 and 0.0020, respectively. The results suggested that the linear effect of  $X_1$ ,  $X_2$  and  $X_3$  on COD removal was significant, indicating that the three factors effect COD removal significantly in an order of catalyst dosage > PMS dosage > initial pH value [12]. In summary, we can conclude that the polynomial regression model can well predict COD removal from coking wastewater by the  $\alpha$ -MnO<sub>2</sub>/PMS process.

**Table 1.** Analysis of variance for the response surface optimization.

Source	Sum of Squares	df	Mean Square	F Value	p Value	
Model	5351.403	9	594.600	17.451	0.0005	significant
$X_1$	4465.125	1	4465.125	131.051	<0.0001	
$X_2$	782.101	1	782.101	79.751	0.0008	
$X_3$	25.600	1	25.600	22.955	0.0020	
$X_1 X_2$	21.160	1	21.160	0.621	0.4565	
$X_1 X_3$	0.010	1	0.010	0.001	0.9868	
$X_2 X_3$	26.523	1	26.523	0.778	0.4069	

**Table 1.** *Cont.*

Source	Sum of Squares	df	Mean Square	F Value	p Value	
$X_1^2$	0.022	1	0.022	0.001	0.9803	
$X_2^2$	20.788	1	20.788	0.610	0.4603	
$X_3^2$	14.933	1	14.9338	0.438	0.5291	
Residual	238.502	7	34.072			
Lack of Fit	238.495	5	47.699	7.660	0.2154	not significant
Pure Error	0.007	2	0.003			
Cor Total	5589.905	16				

**Table 2.** Results of error statistical analysis.

R-Squared	Mean	Adj R-Squared	C.V.%	Pred R-Squared	PRESS	Adeq Precisor
0.9874	58.21	0.9626	3.7	0.7007	2791.36	14.977

The RSM 3D response contour maps of COD removal and their corresponding contour maps are provided in Figure 5. In the 3D response contour maps which evaluate the interaction among the response variable and the two factors, the interaction was stronger when the maps were steeper [69]. The map formed a good “slope” surface in Figure 5A, suggesting the dosage of catalyst and the dosage of PMS had significant effects on COD removal. From the contour map (Figure 5B), we found that COD removal increased monotonously along with the increase in the dosage of catalyst and that of PMS. In addition, the increase in the dosage of catalyst was more significant to the increase in COD removal than the increase in the dosage of PMS. In Figure 5C, a good “slope” surface was also illustrated. However, in the contour map (Figure 5D), we found that COD removal increased along with the increase in initial pH in the window of 3.0 to 6.5 and then decreased when the initial pH further increased. The results were similar with those in phenol removal assays (*vide supra* in Figure 1B). In Figure 5E, indicating the interaction among the COD removal, the dosage of PMS and the initial pH, the 3D map became much gentler. The results once again proved that the dosage of catalyst is the most important factor to manipulate COD removal from coking wastewater [70]. In the contour map (Figure 5F), the initial pH of 6.5 was once again proved as the optimal pH value for COD removal. Based on the RSM 3D response contour maps and the model, we identified the optimal parameters for the  $\alpha$ -MnO<sub>2</sub>/PMS process to remove COD from coking wastewater to be 50 g/L catalyst, 50 mM PMS and an initial pH of 6.5. Under the aforementioned reaction condition, COD removal of 74.6% was predicted to be achieved.

Based on the aforementioned achievements, some issues on the policies for the disposal and discharge of coking wastewater can be suggested. Firstly, AOPs via a non-radical mechanism can be listed as one of the standard technologies or technology units combined with traditional ones to dispose coking wastewater. Secondly, concentrations of impurities in wastewater, especially that of phosphate, should be carefully controlled in the influence of AOPs technologies. Last but not least, the yield of potential toxic degradation intermediates or products in the effluent also need to be carefully controlled.

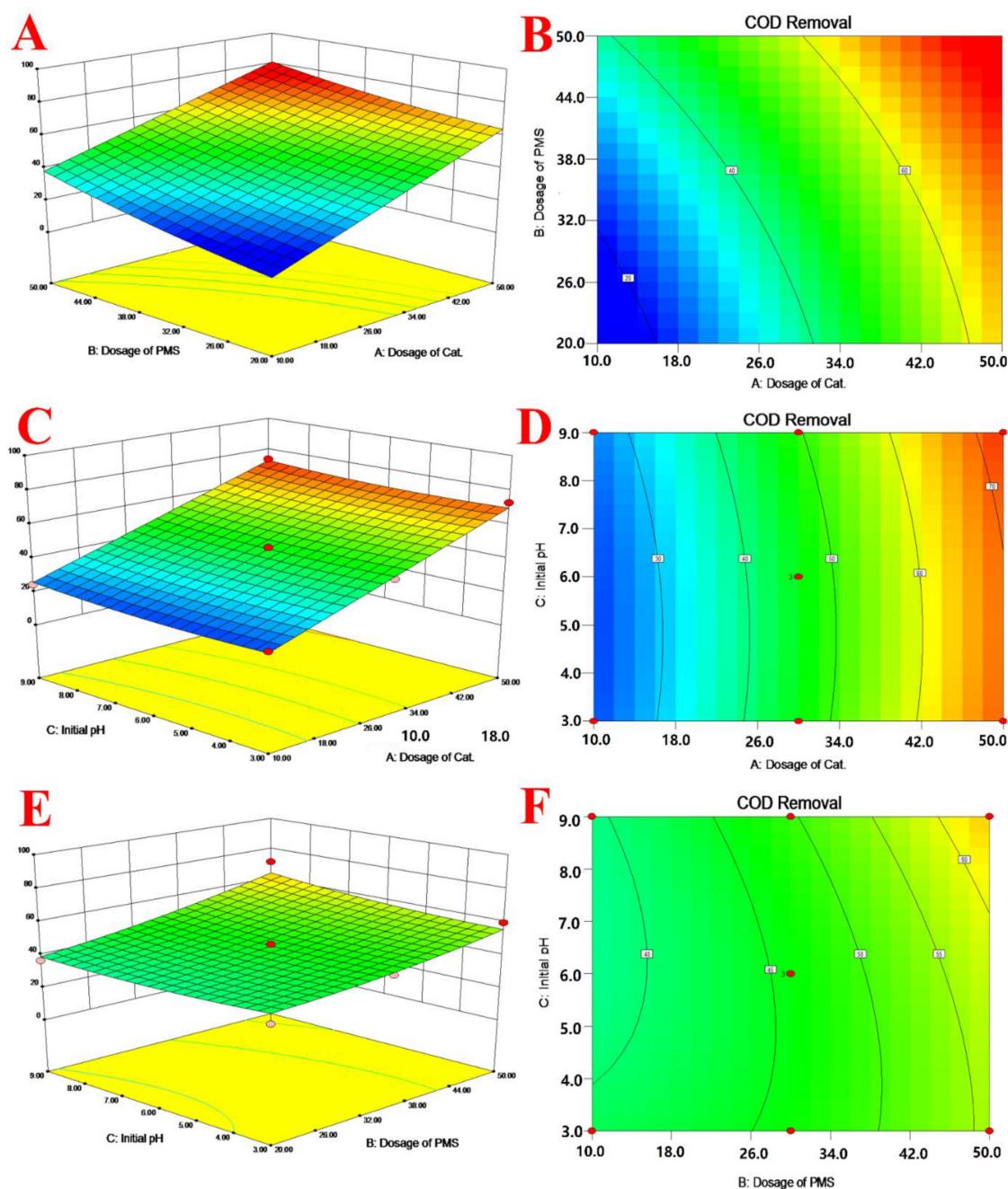


**Figure 5.** 3D response surface contour of COD removal between the dosage of Cat. and the dosage of PMS (A), the dosage of Cat. and initial pH (C), the dosage of PMS and initial pH (E) and the corresponding contour maps (B,D,F).

### 3. Materials and Methods

#### 3.1. Materials

The coking wastewater was collected locally in Hubei Province, PR China. Its physico-chemical properties are provided in Table 3.  $\alpha$ -MnO<sub>2</sub> was synthesized via the procedure described in our previous work [34]. The details can be found in Text S1. Tap and lake water were sampled in the campus of Huazhong University of Science and Technology, Wuhan, P.R. China. Their physico-chemical properties are provided in Tables S2 and S3, respectively.

**Table 3.** Physicochemical properties of the coking wastewater.

Parameters	Values *
pH value	7.17 ± 0.25
Electrical Conductivity (mS/cm)	13.46 ± 0.97
Alkalinity (mg CaCO <sub>3</sub> /L)	3349.00 ± 102.37
COD (mg/L)	1135.00 ± 47.90
BOD <sub>5</sub> (mg/L)	195.00 ± 16.30
TOC (mg/L)	298.45 ± 21.40
Total phenol (mg/L)	377.35 ± 37.80
CN <sup>-</sup> (mg/L)	83.20 ± 14.60
SCN <sup>-</sup> (mg/L)	115.70 ± 19.80
Cl <sup>-</sup> (mg/L)	297.40 ± 31.20
NH <sub>4</sub> <sup>+</sup> -N (mg/L)	178.50 ± 11.90
Total nitrogen (mg/L)	276.60 ± 24.80

\* Value ± standard deviation.

### 3.2. Chemicals

Ultrapure water (18.0 MΩ cm) used in all experiments was produced by a Millipore Milli-Q system (USA). Potassium permanganate (KMnO<sub>4</sub>), manganese sulfate (MnSO<sub>4</sub>), sodium phosphate (Na<sub>3</sub>PO<sub>4</sub>), nitric acid (HNO<sub>3</sub>), sodium hydroxide (NaOH), sodium carbonate (Na<sub>2</sub>CO<sub>3</sub>), sodium bicarbonate (NaHCO<sub>3</sub>), sodium sulfate (Na<sub>2</sub>SO<sub>4</sub>), sodium nitrate (NaNO<sub>3</sub>) and sodium chloride (NaCl) were purchased from Sinopharm Chemical Reagent Co., Ltd. (Shanghai, China). Peroxymonosulfate (PMS, KHSO<sub>5</sub>·0.5KHSO<sub>4</sub>·0.5K<sub>2</sub>SO<sub>4</sub>, 47%), phenol, humic acid (HA), tert-butyl alcohol (TBA), methanol (MeOH, CH<sub>3</sub>OH), furfuryl alcohol (FFA), acetonitrile, N-diethyl-p-phenylenediamine (DPD), deuterated water (D<sub>2</sub>O) 5,5-dimethylpyrrolidineN-oxide (DMPO), 2,2,6,6-tetramethyl-4-piperidinol (TEMP) and methyl phenyl sulfoxide (PMSO) were obtained from Adamas Reagent Co. All chemicals and reagents in this study were of analytical grade and used without further purification.

### 3.3. Characterization of α-MnO<sub>2</sub>

The X-ray diffraction (XRD) data were obtained using an 08 x'pert3 powder diffractometer with graphite monochromatized Cu Kα radiation. The structure and morphology were examined with a SEM (ZEISS Gemini 300, Carl Zeiss AG, Oberkochen, Baden-Württemberg, Germany). Furthermore, a zeta potential analyzer (Nanotracer Wave, Microtrac, Montgomeryville, PA, USA) was performed to record the surface charge of catalysts in water. The metal ions leaching was measured by inductive coupled plasma-optical emission spectrometry (ICP-OES, Optima 8300, PerkinElmer, Waltham, MA, USA). Electrochemical experiments were plotted on a CHI760 Electrochemical workstation (78738, CH Instrument Company, Austin, TX, USA) using a standard three-electrode cell (glassy carbon electrode as the working electrode, Ag/AgCl (4 M KCl) as a reference electrode and platinum wire electrode as a counter electrode). The solution containing 5.0 mM [Fe(CN)<sub>6</sub>]<sup>3-</sup>/<sup>4-</sup> and 0.1 M KCl was selected as the electrolyte solution. Firstly, the mixture of 20 mg of α-MnO<sub>2</sub>, 0.2 mL of Nafion (5 wt%) and 2 mL EtOH was sonicated for an hour. Afterwards, 20 mL of the mixture was dropped on the glassy carbon electrode and dried in a 60 °C vacuum oven.

### 3.4. Experiments to Remove Phenol

Assays to remove phenol were performed in a 100 mL glass beaker which was placed in a water bath at 30 °C with constant magnetic stirring. In a typical procedure, 20 mL of phenol stock solution was transferred to the beaker, followed by the injection of catalyst and PMS. Initial pH was immediately adjusted by nitric acid and sodium hydroxide if needed. Subsequently, 1 mL of the reaction solution was withdrawn at predetermined time intervals and analyzed immediately after being filtered through a 0.22 μm nylon filter. All experiments were performed in triplicate.

### 3.5. Experiments to Treat Coking Wastewater

Assays to treat coking wastewater were conducted in a 500 mL glass beaker in a water bath at 30 °C with constant magnetic stirring. In a typical procedure, 250 mL of coking wastewater was transferred to the beaker, followed by the injection of the catalyst and PMS. The initial pH was immediately adjusted by nitric acid and sodium hydroxide if needed. Subsequently, 10 mL of the coking wastewater was withdrawn at predetermined time intervals and analyzed immediately after being filtered through a 0.22 µm nylon filter. All experiments were performed in triplicate.

To find out how the reaction conditions effects COD removal, the three key parameters including catalyst dosage, PMS dosage and initial pH were selected to develop the prediction model. Based on the data from seventeen sets of preliminary experiments, the RSM model combined with the Box–Behnken experimental design (BBD) was employed to design the experiment sets and optimize COD removal by our system. All the RSM results were analyzed by Design Expert Program (Version 13.0.0.0).

### 3.6. Analytic Technologies

The concentration of phenol was determined by a high-performance liquid chromatography (HPLC-Agilent 1200) with C18 column and ultraviolet (UV) detector. Acetonitrile (15%) and ultra-pure water (85%) at a flow rate of 1 mL/min were used as the mobile phase. A detection wavelength of 254 nm was used to analyze the concentration. For electrochemical studies, the powdered catalysts were first dispersed in ethanol. A droplet of highly disperse catalyst (5 µL) was dropped onto the glassy electrode and then dried at 105 °C. This procedure was repeated three times. Quenching studies, EPR tests and PMSO oxidation experiments were carried out to identify the dominated ROS. Details can be found in Text S2. The concentration of PMS was examined by the DPD method [71]. Details can be found in Text S3. COD was evaluated by the dichromate method in accordance with the standard methods issued by the China National Environmental Protection Agency [72]. BOD<sub>5</sub> was measured using a BOD analyzer (Trak TM II, Hach Co., Loveland, CO, USA). pH was measured using a pH meter (Hach Sension 1, Hach Co., Loveland, CO, USA).

## 4. Conclusions

A  $\alpha$ -MnO<sub>2</sub>/PMS process was employed to efficiently dispose coking wastewater in this study. ROS including sulfate radicals, hydroxyl radicals, superoxide radicals and singlet oxygen were ruled out as contributors to degrade organic matter. PMS mediated electron transfer was identified as the major mechanism of organic degradation. Favored by the electron transfer mechanism, water parameters including initial pH, common anions and natural organic matters showed limited effects on the degradation reaction. In the treatment of coking wastewater, a satisfying COD removal of 73.8% of COD was removed within 180 min of reaction with 50 g/L  $\alpha$ -MnO<sub>2</sub> and 50 mM PMS at pH<sub>0</sub> 7.0. Furthermore, the biodegradability of coking wastewater was remarkably enhanced due to BOD<sub>5</sub>/COD increasing from 0.172 to 0.419 after the treatment. The reuse performance was good as COD removal decreased only 1.1% after the five-time cycle application. Employing COD removal as the dependent variable, a quadratic polynomial regression model was further built to optimize the reaction conditions. By the model, we found the dosage of  $\alpha$ -MnO<sub>2</sub> as the most important parameters to enhance the performance. The optimal reaction conditions were identified as 50 g/L  $\alpha$ -MnO<sub>2</sub>, 50 mM PMS and pH<sub>0</sub> 6.5 by the model. Under such reaction conditions, COD removal of 74.6% was predicted to be achieved. By all aforementioned efforts,  $\alpha$ -MnO<sub>2</sub>/PMS process was proved as a promising technology for the disposal of coking wastewater and supported its potential full-scale application.

**Supplementary Materials:** The following supporting information can be downloaded at: <https://www.mdpi.com/article/10.3390/catal12111359/s1>, Text S1: Details of synthesis procedures of  $\alpha$ -MnO<sub>2</sub>; Text S2: Identification of dominated ROS; Text S3: Details of the detection of PMS concentration; Figure S1: SEM image of  $\alpha$ -MnO<sub>2</sub>; Figure S2: XRD pattern of  $\alpha$ -MnO<sub>2</sub>; Figure S3: Zeta potential in the

pH range from 3.0 to 11.0; Figure S4: Leaching of Mn in pH window of 3.0 to 9.0; Figure S5: Formation of  $\text{BrO}_3^-$  in the presence of  $\text{Br}^-$ ; Figure S6: Removal of phenol by  $\alpha\text{-MnO}_2/\text{PMS}$  system in deionized water, tap water or lake water; Figure S7: Phenol removal in  $\text{D}_2\text{O}$  and deionized water and first-order kinetic model fitting results of the phenol removal; Table S1: Box-Behnken design and results of COD removal; Table S2: Physico-chemical properties of the tap water; Table S3: Physico-chemical properties of the lake water. Reference [34] is cited in the Supplementary Materials.

**Author Contributions:** J.W.: Data curation, Methodology, Validation, Investigation, Visualization, Writing—original draft; Z.L.: Investigation; J.C.: Data curation; S.W. (Siqi Wang): Data curation; F.L.: Methodology; J.I.: Investigation; S.W. (Songlin Wang): Methodology; X.Z.: Methodology, Project administration, Supervision, Writing—review & editing; Z.C.: Conceptualization, Funding acquisition, Project administration, Supervision, Writing—review & editing. All authors have read and agreed to the published version of the manuscript.

**Funding:** This work was financially supported by the National Key R&D Program of China (No. 2018YFC1802302), the National Science Foundation of China (No. 52200154), the Fundamental Research Funds for the Central Universities (No. 2019kfyRCPY058), Chutian Scholar Foundation from Hubei Province, Program for HUST Academic Frontier Youth Team, and Innovative Research Post for Postdoctor from Hubei Province.

**Acknowledgments:** We thanks the Analytical and Testing Centre of Huazhong University of Science and Technology for the help of the characterization of  $\alpha\text{-MnO}_2$ .

**Conflicts of Interest:** The authors declare that they have no known competing financial interests or personal relationships that could have appeared to influence the work reported in this paper.

## References

1. Deng, F.; Qiu, S.; Zhu, Y.; Zhang, X.; Yang, J.; Ma, F. Tripolyphosphate-assisted electro-Fenton process for coking wastewater treatment at neutral pH. *Environ. Sci. Pollut. Res.* **2019**, *26*, 11928–11939. [[CrossRef](#)] [[PubMed](#)]
2. Wang, S.; Wang, J. Treatment of membrane filtration concentrate of coking wastewater using PMS/chloridion oxidation process. *Chem. Eng. J.* **2020**, *379*, 122361. [[CrossRef](#)]
3. Ghosh, T.K.; Biswas, P.; Bhunia, P.; Kadukar, S.; Banerjee, S.K.; Ghosh, R.; Sarkar, S. Application of coke breeze for removal of colour from coke plant wastewater. *J. Environ. Manag.* **2022**, *302*, 113800. [[CrossRef](#)] [[PubMed](#)]
4. Pitas, V.; Somogyi, V.; Karpati, A.; Thury, P.; Frater, T. Reduction of chemical oxygen demand in a conventional activated sludge system treating coke oven wastewater. *J. Clean. Prod.* **2020**, *273*, 122482. [[CrossRef](#)]
5. Ren, G.; Zhou, M.; Zhang, Q.; Xu, X.; Li, Y.; Su, P.; Paidar, M.; Bouzek, K. Cost-efficient improvement of coking wastewater biodegradability by multi-stages flow through peroxi-coagulation under low current load. *Water Res.* **2019**, *154*, 336–348. [[CrossRef](#)] [[PubMed](#)]
6. Wang, C.; Liu, Y.; Huang, M.; Xiang, W.; Wang, Z.; Wu, X.; Zan, F.; Zhou, T. A rational strategy of combining Fenton oxidation and biological processes for efficient nitrogen removal in toxic coking wastewater. *Bioresour. Technol.* **2022**, *363*, 127897. [[CrossRef](#)]
7. Chen, B.; Yang, S.; Wu, Y.; Suo, M.; Qian, Y. Intensified phenols extraction and oil removal for industrial semi-coking wastewater: A novel economic pretreatment process design. *J. Clean. Prod.* **2020**, *242*, 118453.
8. Liu, Z.; Teng, Y.; Xu, Y.; Zheng, Y.; Zhang, Y.; Zhu, M.; Sun, Y. Ozone catalytic oxidation of biologically pretreated semi-coking wastewater (BPSCW) by spinel-type  $\text{MnFe}_2\text{O}_4$  magnetic nanoparticles. *Sep. Purif. Technol.* **2022**, *278*, 118277.
9. Sun, G.; Zhang, Y.; Gao, Y.; Han, X.; Yang, M. Removal of hard COD from biological effluent of coking wastewater using synchronized oxidation-adsorption technology: Performance, mechanism, and full-scale application. *Water Res.* **2020**, *173*, 115517. [[CrossRef](#)]
10. Cui, Y.; Kang, W.; Qin, L.; Ma, J.; Liu, X.; Yang, Y. Magnetic surface molecularly imprinted polymer for selective adsorption of quinoline from coking wastewater. *Chem. Eng. J.* **2020**, *397*, 125480. [[CrossRef](#)]
11. Yuan, R.; Xia, Y.; Wu, X.; He, C.; Qin, Y.; He, C.; Zhang, X.; Li, N.; He, X. Efficient advanced treatment of coking wastewater using  $\text{O}_3/\text{H}_2\text{O}_2/\text{Fe}$ -shavings process. *J. Environ. Chem. Eng.* **2022**, *10*, 107307. [[CrossRef](#)]
12. Hu, Y.; Yu, F.; Bai, Z.; Wang, Y.; Zhang, H.; Gao, X.; Wang, Y.; Li, X. Preparation of Fe-loaded needle coke particle electrodes and utilisation in three-dimensional electro-Fenton oxidation of coking wastewater. *Chemosphere* **2022**, *308*, 136544. [[CrossRef](#)]
13. Zhou, X.; Hou, Z.; Lv, L.; Song, J.; Yin, Z. Electro-Fenton with peroxi-coagulation as a feasible pre-treatment for high-strength refractory coke plant wastewater: Parameters optimization, removal behavior and kinetics analysis. *Chemosphere* **2020**, *238*, 124649. [[CrossRef](#)]
14. Tamang, M.; Paul, K.K. Advances in treatment of coking wastewater—A state of art review. *Water Sci. Technol.* **2022**, *85*, 449–473. [[CrossRef](#)]
15. Iskurt, C.; Keyikoglu, R.; Kobya, M.; Khataee, A. Treatment of coking wastewater by aeration assisted electrochemical oxidation process at controlled and uncontrolled initial pH conditions. *Sep. Purif. Technol.* **2020**, *248*, 117043. [[CrossRef](#)]

16. Wang, J.; Cai, J.; Wang, S.; Zhou, X.; Ding, X.; Ali, J.; Zheng, L.; Wang, S.; Yang, L.; Xi, S.; et al. Biochar-based activation of peroxide: Multivariate-controlled performance, modulatory surface reactive sites and tunable oxidative species. *Chem. Eng. J.* **2022**, *428*, 131233. [[CrossRef](#)]
17. An, W.; Wang, H.; Yang, T.; Xu, J.; Wang, Y.; Liu, D.; Hu, J.; Cui, W.; Liang, Y. Enriched photocatalysis-Fenton synergistic degradation of organic pollutants and coking wastewater via surface oxygen vacancies over Fe-BiOBr composites. *Chem. Eng. J.* **2023**, *451*, 138653. [[CrossRef](#)]
18. Verma, V.; Chaudhari, P.K. Optimization of multiple parameters for treatment of coking wastewater using Fenton oxidation. *Arab. J. Chem.* **2020**, *13*, 5084–5095. [[CrossRef](#)]
19. Razaviarani, V.; Zazo, J.A.; Casas, J.A.; Jaffe, P.R. Coupled fenton-denitrification process for the removal of organic matter and total nitrogen from coke plant wastewater. *Chemosphere* **2019**, *224*, 653–657. [[CrossRef](#)]
20. Kang, J.; Liu, Z.; Yu, C.; Wang, Y.; Wang, X. Degradation performance of high-concentration coking wastewater by manganese oxide ore acidic oxidation. *Water Sci. Technol.* **2022**, *86*, 367–379. [[CrossRef](#)]
21. Wang, J.; Gong, Q.; Ali, J.; Shen, M.; Cai, J.; Zhou, X.; Liao, Z.; Wang, S.; Chen, Z. pH-dependent transformation products and residual toxicity evaluation of sulfamethoxazole degradation through non-radical oxygen species involved process. *Chem. Eng. J.* **2020**, *390*, 124512. [[CrossRef](#)]
22. Yang, L.; Jiao, Y.; Xu, X.; Pan, Y.; Su, C.; Duan, X.; Sun, H.; Liu, S.; Wang, S.; Shao, Z. Superstructures with Atomic-Level Arranged Perovskite and Oxide Layers for Advanced Oxidation with an Enhanced Non-Free Radical Pathway. *ACS Sustain. Chem. Eng.* **2022**, *10*, 1899–1909. [[CrossRef](#)]
23. Zeng, Z.; Khan, A.; Wang, Z.; Zhao, M.; Mo, W.; Chen, Z. Elimination of atrazine through radical/non-radical combined processes by manganese nano-catalysts/PMS and implications to the structure-performance relationship. *Chem. Eng. J.* **2020**, *397*, 125425. [[CrossRef](#)]
24. Wang, J.; Liao, Z.; Ifthikar, J.; Shi, L.; Chen, Z.; Chen, Z. One-step preparation and application of magnetic sludge-derived biochar on acid orange 7 removal via both adsorption and persulfate based oxidation. *RSC Adv.* **2017**, *7*, 18696–18706. [[CrossRef](#)]
25. Wang, J.; Liao, Z.; Ifthikar, J.; Shi, L.; Du, Y.; Zhu, J.; Xi, S.; Chen, Z.; Chen, Z. Treatment of refractory contaminants by sludge-derived biochar/persulfate system via both adsorption and advanced oxidation process. *Chemosphere* **2017**, *185*, 754–763. [[CrossRef](#)]
26. Wang, J.; Shen, M.; Wang, H.; Du, Y.; Zhou, X.; Liao, Z.; Wang, H.; Chen, Z. Red mud modified sludge biochar for the activation of peroxymonosulfate: Singlet oxygen dominated mechanism and toxicity prediction. *Sci. Total Environ.* **2020**, *740*, 140388. [[CrossRef](#)]
27. Wang, J.; Shen, M.; Gong, Q.; Wang, X.; Cai, J.; Wang, S.; Chen, Z. One-step preparation of ZVI-sludge derived biochar without external source of iron and its application on persulfate activation. *Sci. Total Environ.* **2020**, *714*, 136728.
28. Guo, Z.Y.; Li, C.X.; Gao, M.; Han, X.; Zhang, Y.J.; Zhang, W.J.; Li, W.W. Mn-O Covalency Governs the Intrinsic Activity of Co-Mn Spinel Oxides for Boosted Peroxymonosulfate Activation. *Angew. Chem. Int. Ed.* **2021**, *60*, 274–280. [[CrossRef](#)]
29. Kuang, H.; He, Z.; Li, M.; Huang, R.; Zhang, Y.; Xu, X.; Wang, L.; Chen, Y.; Zhao, S. Enhancing co-catalysis of MoS<sub>2</sub> for persulfate activation in Fe<sup>3+</sup>-based advanced oxidation processes via defect engineering. *Chem. Eng. J.* **2021**, *417*, 127987.
30. Shao, P.; Jing, Y.; Duan, X.; Lin, H.; Yang, L.; Ren, W.; Deng, F.; Li, B.; Luo, X.; Wang, S. Revisiting the Graphitized Nanodiamond-Mediated Activation of Peroxymonosulfate: Singlet Oxygenation versus Electron Transfer. *Environ. Sci. Technol.* **2021**, *55*, 16078–16087.
31. Wu, L.; Sun, Z.; Zhen, Y.; Zhu, S.; Yang, C.; Lu, J.; Tian, Y.; Zhong, D.; Ma, J. Oxygen Vacancy-Induced Nonradical Degradation of Organics: Critical Trigger of Oxygen (O-2) in the Fe-Co LDH/Peroxymonosulfate System. *Environ. Sci. Technol.* **2021**, *55*, 15400–15411. [[CrossRef](#)]
32. Xu, X.; Zhang, Y.; Zhou, S.; Huang, R.; Huang, S.; Kuang, H.; Zeng, X.; Zhao, S. Activation of persulfate by MnOOH: Degradation of organic compounds by nonradical mechanism. *Chemosphere* **2021**, *272*, 129629. [[CrossRef](#)]
33. Jawad, A.; Zhan, K.; Wang, H.; Shahzad, A.; Zeng, Z.; Wang, J.; Zhou, X.; Ullah, H.; Chen, Z.; Chen, Z. Tuning of Persulfate Activation from a Free Radical to a Nonradical Pathway through the Incorporation of Non-Redox Magnesium Oxide. *Environ. Sci. Technol.* **2020**, *54*, 2476–2488. [[CrossRef](#)]
34. Shen, S.; Zhou, X.; Zhao, Q.; Jiang, W.; Wang, J.; He, L.; Ma, Y.; Yang, L.; Chen, Z. Understanding the nonradical activation of peroxymonosulfate by different crystallographic MnO<sub>2</sub>: The pivotal role of Mn-III content on the surface. *J. Hazard. Mater.* **2022**, *439*, 129613. [[CrossRef](#)]
35. Wang, Y.; Zhang, Z.; Yin, Z.; Liu, Z.; Liu, Y.; Yang, Z.; Yang, W. Adsorption and catalysis of peroxymonosulfate on carbocatalysts for phenol degradation: The role of pyrrolic-nitrogen. *Appl. Catal. B Environ.* **2022**, *319*, 121891. [[CrossRef](#)]
36. Wang, W.; Liu, Y.; Yue, Y.; Wang, H.; Cheng, G.; Gao, C.; Chen, C.; Ai, Y.; Chen, Z.; Wang, X. The Confined Interlayer Growth of Ultrathin Two-Dimensional Fe<sub>3</sub>O<sub>4</sub> Nanosheets with Enriched Oxygen Vacancies for Peroxymonosulfate Activation. *ACS Catal.* **2021**, *11*, 11256–11265. [[CrossRef](#)]
37. Pan, J.; Gao, B.; Duan, P.; Guo, K.; Akram, M.; Xu, X.; Yue, Q.; Gao, Y. Improving peroxymonosulfate activation by copper ion-saturated adsorbent-based single atom catalysts for the degradation of organic contaminants: Electron-transfer mechanism and the key role of Cu single atoms. *J. Mater. Chem. A* **2021**, *9*, 11604–11613. [[CrossRef](#)]

38. Chen, F.; Liu, L.L.; Chen, J.J.; Li, W.W.; Chen, Y.P.; Zhang, Y.J.; Wu, J.H.; Mei, S.C.; Yang, Q.; Yu, H.Q. Efficient decontamination of organic pollutants under high salinity conditions by a nonradical peroxymonosulfate activation system. *Water Res.* **2021**, *191*, 116799. [[CrossRef](#)]
39. Zhou, X.; Zhao, Q.; Wang, J.; Chen, Z.; Chen, Z. Nonradical oxidation processes in PMS-based heterogeneous catalytic system: Generation, identification, oxidation characteristics, challenges response and application prospects. *Chem. Eng. J.* **2021**, *410*, 128312. [[CrossRef](#)]
40. Kohantorabi, M.; Moussavi, G.; Giannakis, S. A review of the innovations in metal- and carbon-based catalysts explored for heterogeneous peroxymonosulfate (PMS) activation, with focus on radical vs non-radical degradation pathways of organic contaminants. *Chem. Eng. J.* **2021**, *411*, 127957. [[CrossRef](#)]
41. Yang, Y.; Zhang, P.; Hu, K.; Zhou, P.; Wang, Y.; Asif, A.H.; Duan, X.; Sun, H.; Wang, S. Crystallinity and valence states of manganese oxides in Fenton-like polymerization of phenolic pollutants for carbon recycling against degradation. *Appl. Catal. B Environ.* **2022**, *315*, 121593. [[CrossRef](#)]
42. Fu, J.; Gao, P.; Wang, L.; Zhang, Y.; Deng, Y.; Huang, R.; Zhao, S.; Yu, Z.; Wei, Y.; Wang, G.; et al. Regulating Crystal Facets of MnO<sub>2</sub> for Enhancing Peroxymonosulfate Activation to Degrade Pollutants: Performance and Mechanism. *Catalysts* **2022**, *12*, 342. [[CrossRef](#)]
43. Liu, F.; Wang, Z.; You, S.; Liu, Y. Electrogenated quinone intermediates mediated peroxymonosulfate activation toward effective water decontamination and electrode antifouling. *Appl. Catal. B Environ.* **2023**, *320*, 121980. [[CrossRef](#)]
44. Wang, Z.; Almatrafi, E.; Wang, H.; Qin, H.; Wang, W.; Du, L.; Chen, S.; Zeng, G.; Xu, P. Cobalt Single Atoms Anchored on Oxygen-Doped Tubular Carbon Nitride for Efficient Peroxymonosulfate Activation: Simultaneous Coordination Structure and Morphology Modulation. *Angew. Chem. Int. Ed.* **2022**, *61*, e202202338.
45. Zhou, X.; Luo, C.; Wang, J.; Wang, H.; Chen, Z.; Wang, S.; Chen, Z. Recycling application of modified waste electrolytic manganese anode slag as efficient catalyst for PMS activation. *Sci. Total Environ.* **2021**, *762*, 143120. [[CrossRef](#)]
46. Zhou, X.; Zhao, Q.; Tian, Y.; Wang, J.; Jawad, A.; Wang, S.; Chen, Z.; Chen, Z. Identification of step-by-step oxidation process and its driving mechanism in the peroxymonosulfate catalytically activated with redox metal oxides. *Chem. Eng. J.* **2022**, *436*, 131256. [[CrossRef](#)]
47. Zhou, X.; Zhao, Q.; Wang, J.; Wei, X.; Zhang, R.; Wang, S.; Liu, P.; Chen, Z. Effects of foreign metal doping on the step-by-step oxidation process in M-OMS-2 catalyzed activation of PMS. *J. Hazard. Mater.* **2022**, *434*, 128773. [[CrossRef](#)]
48. Oyekunle, D.T.; Cai, J.; Gendy, E.A.; Chen, Z. Impact of chloride ions on activated persulfates based advanced oxidation process (AOPs): A mini review. *Chemosphere* **2021**, *280*, 130949. [[CrossRef](#)]
49. Wu, Y.; Yang, Y.; Liu, Y.; Zhang, L.; Feng, L. Modelling study on the effects of chloride on the degradation of bezafibrate and carbamazepine in sulfate radical-based advanced oxidation processes: Conversion of reactive radicals. *Chem. Eng. J.* **2019**, *358*, 1332–1341. [[CrossRef](#)]
50. Duan, P.; Liu, X.; Liu, B.; Akram, M.; Li, Y.; Pan, J.; Yue, Q.; Gao, B.; Xu, X. Effect of phosphate on peroxymonosulfate activation: Accelerating generation of sulfate radical and underlying mechanism. *Appl. Catal. B Environ.* **2021**, *298*, 120532. [[CrossRef](#)]
51. Li, H.; Yuan, N.; Qian, J.; Pan, B. Mn<sub>2</sub>O<sub>3</sub> as an Electron Shuttle between Peroxymonosulfate and Organic Pollutants: The Dominant Role of Surface Reactive Mn(IV) Species. *Environ. Sci. Technol.* **2022**, *56*, 4498–4506. [[CrossRef](#)]
52. Yang, J.; Dong, Z.; Jiang, C.; Wang, C.; Liu, H. An overview of bromate formation in chemical oxidation processes: Occurrence, mechanism, influencing factors, risk assessment, and control strategies. *Chemosphere* **2019**, *237*, 124521. [[CrossRef](#)]
53. Appiani, E.; Ossola, R.; Latch, D.E.; Erickson, P.R.; McNeill, K. Aqueous singlet oxygen reaction kinetics of furfuryl alcohol: Effect of temperature, pH, and salt content. *Environ. Sci. Proc. Imp.* **2017**, *19*, 507–516. [[CrossRef](#)]
54. Zhu, S.; Li, X.; Kang, J.; Duan, X.; Wang, S. Persulfate Activation on Crystallographic Manganese Oxides: Mechanism of Singlet Oxygen Evolution for Nonradical Selective Degradation of Aqueous Contaminants. *Environ. Sci. Technol.* **2019**, *53*, 307–315. [[CrossRef](#)]
55. Hu, Y.; Sun, S.; Guo, J.; Cheng, F.; Li, Z. In situ anchoring strategy to enhance dual nonradical degradation of sulfamethoxazole with high loading manganese doped carbon nitride. *Chemosphere* **2022**, *303*, 135035. [[CrossRef](#)]
56. Sun, W.; Pang, K.; Ye, F.; Pu, M.; Zhou, C.; Huang, H.; Zhang, Q.; Niu, J. Carbonization of camphor sulfonic acid and melamine to N,S-co-doped carbon for sulfamethoxazole degradation via persulfate activation: Nonradical dominant pathway. *Sep. Purif. Technol.* **2021**, *279*, 119723. [[CrossRef](#)]
57. Wang, L.; Xu, H.; Jiang, N.; Pang, S.; Jiang, J.; Zhang, T. Effective activation of peroxymonosulfate with natural manganese-containing minerals through a nonradical pathway and the application for the removal of bisphenols. *J. Hazard. Mater.* **2021**, *417*, 126152. [[CrossRef](#)]
58. Shahzad, A.; Ali, J.; Ifthikar, J.; Aregay, G.G.; Zhu, J.; Chen, Z.; Chen, Z. Non-radical PMS activation by the nanohybrid material with periodic confinement of reduced graphene oxide (rGO) and Cu hydroxides. *J. Hazard. Mater.* **2020**, *392*, 122316.
59. Jiang, N.; Xu, H.; Wang, L.; Jiang, J.; Zhang, T. Nonradical Oxidation of Pollutants with Single-Atom-Fe(III)-Activated Persulfate: Fe(V) Being the Possible Intermediate Oxidant. *Environ. Sci. Technol.* **2020**, *54*, 14057–14065.
60. Wang, Z.; Jiang, J.; Pang, S.; Zhou, Y.; Guan, C.; Gao, Y.; Li, J.; Yang, Y.; Qu, W.; Jiang, C. Is Sulfate Radical Really Generated from Peroxydisulfate Activated by Iron(II) for Environmental Decontamination? *Environ. Sci. Technol.* **2018**, *52*, 11276–11284.
61. Ren, W.; Nie, G.; Zhou, P.; Zhang, H.; Duan, X.; Wang, S. The Intrinsic Nature of Persulfate Activation and N-Doping in Carbocatalysis. *Environ. Sci. Technol.* **2020**, *54*, 6438–6447. [[CrossRef](#)] [[PubMed](#)]

62. Wang, L.; Wang, Y.; Zhang, L.; Li, T.; Yang, M.; Hu, C. CoO anchored on boron nitride nanobelts for efficient removal of water contaminants by peroxymonosulfate activation. *Chem. Eng. J.* **2022**, *430*, 132915. [[CrossRef](#)]
63. Duan, P.; Pan, J.; Du, W.; Yue, Q.; Gao, B.; Xu, X. Activation of peroxymonosulfate via mediated electron transfer mechanism on single-atom Fe catalyst for effective organic pollutants removal. *Appl. Catal. B Environ.* **2021**, *299*, 120714. [[CrossRef](#)]
64. Deng, S.; Jothinathan, L.; Cai, Q.; Li, R.; Wu, M.; Ong, S.L.; Hu, J. FeO<sub>x</sub>@GAC catalyzed microbubble ozonation coupled with biological process for industrial phenolic wastewater treatment: Catalytic performance, biological process screening and microbial characteristics. *Water Res.* **2021**, *190*, 116687. [[CrossRef](#)] [[PubMed](#)]
65. Liu, B.; Guo, W.; Wang, H.; Si, Q.; Zhao, Q.; Luo, H.; Ren, N. B-doped graphitic porous biochar with enhanced surface affinity and electron transfer for efficient peroxydisulfate activation. *Chem. Eng. J.* **2020**, *396*, 125119. [[CrossRef](#)]
66. Yin, C.; Xia, Q.; Zhou, J.; Li, B.; Guo, Y.; Khan, A.; Li, X.; Xu, A. Direct electron transfer process-based peroxymonosulfate activation via surface labile oxygen over mullite oxide YMn<sub>2</sub>O<sub>5</sub> for effective removal of bisphenol A. *Sep. Purif. Technol.* **2022**, *280*, 119924. [[CrossRef](#)]
67. Aram, M.; Farhadian, M.; Nazar, A.R.S.; Tangestaninejad, S.; Eskandari, P.; Jeon, B.-H. Metronidazole and Cephalexin degradation by using of Urea/TiO<sub>2</sub>/ZnFe<sub>2</sub>O<sub>4</sub>/Clinoptilolite catalyst under visible-light irradiation and ozone injection. *J. Mol. Liq.* **2020**, *304*, 112764. [[CrossRef](#)]
68. Turan, N.B.; Erkan, H.S.; Engin, G.O. The investigation of shale gas wastewater treatment by electro-Fenton process: Statistical optimization of operational parameters. *Process Saf. Environ.* **2017**, *109*, 203–213. [[CrossRef](#)]
69. Berkani, M.; Vasseghian, Y.; Le, V.T.; Dragoi, E.-N.; Khaneghah, A.M. The Fenton-like reaction for Arsenic removal from groundwater: Health risk assessment. *Environ. Res.* **2021**, *202*, 111698. [[CrossRef](#)]
70. Chai, Y.; Yang, H.; Bai, M.; Chen, A.; Peng, L.; Yan, B.; Zhao, D.; Qin, P.; Peng, C.; Wang, X. Direct production of 2, 5-Furandicarboxylic acid from raw biomass by manganese dioxide catalysis cooperated with ultrasonic-assisted diluted acid pretreatment. *Bioresour. Technol.* **2021**, *337*, 125421. [[CrossRef](#)]
71. Gokulakrishnan, S.; Mohammed, A.; Prakash, H. Determination of persulphates using N,N-diethyl-p-phenylenediamine as colorimetric reagent: Oxidative coloration and degradation of the reagent without bactericidal effect in water. *Chem. Eng. J.* **2016**, *286*, 223–231. [[CrossRef](#)]
72. Yu, Y.; Chen, Z.; Guo, Z.; Liao, Z.; Yang, L.; Wang, J.; Chen, Z. Removal of Refractory Contaminants in Municipal Landfill Leachate by Hydrogen, Oxygen and Palladium: A Novel Approach of Hydroxyl Radical Production. *J. Hazard. Mater.* **2015**, *287*, 349–355. [[CrossRef](#)]